Progress In Electromagnetics Research, Vol. 140, 91–104, 2013

THE ACCURATE FOURTH-ORDER DOPPLER PARAMETER CALCULATION AND ANALYSIS FOR GEOSYNCHRONOUS SAR

Bingji Zhao[1, *], Xiangyang Qi[1], Hongjun Song[1], Wenjun Gao[2], Xiaolei Han[1], and Runpu Chen[1]

[1]Department of Space Microwave Remote Sensing System, Institute of Electronic, Chinese Academy of Science, Beijing 100190, Republic of China

[2]Beijing Institute of Spacecraft System Engineering, Beijing 100094, Republic of China

Abstract—This paper presents a new approach to calculate the 1–4th order Doppler parameters for Geosynchronous Synthetic Aperture Radar (Geo-SAR). To get accurate calculation results, the Earth is modeled as an ellipsoid and the relative motion between the sensor in an elliptical orbit and the rotating Earth is analyzed. The J_2, J_3 and J_4 orbital perturbation items and attitude steering are analyzed. Ignoring the perturbation force would produce errors of the Doppler parameters for spaceborne SAR because it can influence the six orbital elements. Since the Doppler parameters are related to the antenna beam pointing directions and influenced by attitude of SAR platform, the calculation results before and after attitude steering are shown. Furthermore, the Doppler parameter properties during the whole orbital periods of Geo-SAR are compared with those of Low-Earth-Orbital SAR (Leo-SAR). Finally, the effects on Doppler parameters stemmed from the radar beam pointing accuracy are analyzed.

1. INTRODUCTION

Currently, most of the spaceborne SAR systems are considered as Leo-SAR since they fly at altitudes of 560–870 km. Observation of Earth surface needs large swath widths and short revisit cycle, however, Leo-SAR systems are limited by the low flying altitudes. The Geo-SAR, proposed by Tomiyasu et al., exhibits distinctive advantages which

Received 13 March 2013, Accepted 8 May 2013, Scheduled 22 May 2013

* Corresponding author: Bingji Zhao (zachary_zbj@163.com).

provide an enormous instantaneous field of view with orbital period equal to one Earth day [1–9].

A main problem of it is the super-long integration time to traverse the long non-linear synthetic aperture distance. For example, it needs up to 23 min in some conditions. This is quite different from Leo-SAR. Since a more accurate range model and a different azimuth compression reference function are required for generating high quality images, the 1–4th order Doppler parameters are necessary. Various Doppler parameter calculation algorithms have been reported for Leo-SAR, but show large errors when applied to Geo-SAR due to geometrical approximation [10–13]. Actually, in the satellite case, the geometry is more complicated, as the orbit is elliptical and the Earth is modeled as an ellipsoid rotating independently of the sensor trajectory. An accurate approach of calculating the 1–4th order Doppler parameters in Geo-SAR, which utilizes the data such as the spacecraft ephemeris and attitude, is proposed in this paper.

Furthermore, we analyze the error of Doppler parameter calculation results caused by ignoring orbital perturbation. Due to a variety of perturbing effects, the so-called *six orbital elements* describing the orbit increase or decrease with time, and the satellite orbit could not be considered as an ellipse strictly in an invariant plane. As a result, the state vectors of sensor and target will be different from those in a strict elliptical orbit [15]. As a result, the Doppler parameters, without considering the perturbation force, will not be accurate enough for precision focusing for the spaceborne SAR data. In Leo-SAR condition, the influence from the Earth shape perturbation is the main part. As a result, we analyzes the varieties of the orbital elements under orbital perturbative force when the terms J_2, J_3 and J_4 are all considered, and the values of Doppler parameters are analyzed.

It should be emphasized that the attitude steering is necessary for Geo-SAR. Since the Doppler parameter calculation results depend on the beam pointing considerably, the effects of antenna yaw and pitch on the Doppler parameters are simulated and analyzed. Finally, the beam pointing errors of 0.05° for yaw, pitch and roll angles are assumed, and the effects of pointing errors on the 1–4th order Doppler parameters are illustrated.

This paper is structured as follows. In Section 2, a 3D geometry model is illustrated, and the state vectors of sensor and target are derived based on the model. The 1–4th order Doppler parameter calculation expressions are then advanced. The orbital perturbation is analyzed in Section 3. In Section 4, we discuss the attitude steering. The simulation results are shown in Section 5. Finally, the conclusion is given in Section 6.

2. FOURTH-ORDER DOPPLER PARAMETERS CALCULATION

2.1. Accurate Geometry Model

A satellite's orbit can be described by six orbital elements, which are constants of the ellipse and of its orientation relative to the Earth Centered Inertial coordinate system (ECI). They are: a, the semi-major axis of the orbit; e, the eccentricity of the orbit; θ_i, the inclination of the orbit; Ω, the longitude of the ascending node; ω, the argument of perigee; M, the mean anomaly. As depicted in Fig. 1, consider a satellite local coordinate (SLC) system with origin at the center of the Earth. The X axis of SLC always points to the sensor, the Z axis is perpendicular to the orbital plane, and the Y axis obeys the Cartesian right hand rule. The angle f is true anomaly.

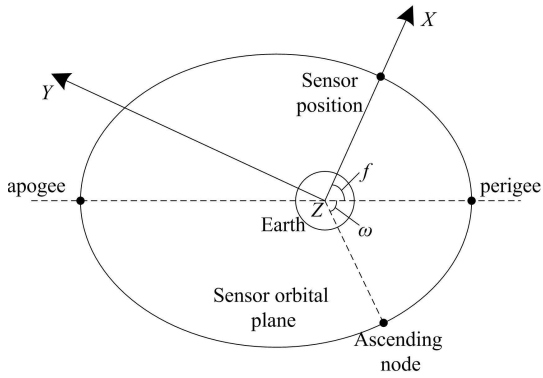

Figure 1. Geo-SAR geometry model in SLC.

To get the 1–4th order Doppler parameters, the 1–5th order state vectors of sensor and target should be presented. The symbols **r**, **v, A, A′ and A″** are respectively the state vectors of position, velocity, acceleration, rate of acceleration, and the second derivative of acceleration. The five state vectors of Geo-SAR can be separately expressed as follows, where the subscript s means satellite:

$$\mathbf{r}_s = (R_s, 0, 0)^T \tag{1}$$

$$\mathbf{v}_s = \sqrt{\mu/[a(1-e^2)]}\,(e\sin f, 1+e\cos f, 0)^T \tag{2}$$

$$\mathbf{A}_s = \left(-\mu/R_s^2, 0, 0\right)^T \tag{3}$$

$$\mathbf{A}'_s = \left(2\mu R'_s/R_s^3, -\mu\omega_s/R_s^2, 0\right)^T \tag{4}$$

$$\mathbf{A}_s{}'' = \left(\frac{2\mu R_s{}'' R_s - 6\mu R_s'^2 + \mu\omega_s^2 R_s^2}{R_s^4}, \quad \frac{4\mu R_s'\omega_s - \mu\omega_s' R_s}{R_s^3}, \quad 0 \right)^T \tag{5}$$

where μ is the gravitational constant, R_s instantaneous distances between sensor and the Earth center, R_s' the first-order temporal derivative of R_s, R_s'' the second-order temporal derivative of R_s, ω_s instantaneous angular velocity of sensor, ω_s' the first-order temporal derivative of ω_s. According to Kepler's second law, R_s, R_s', R_s'', ω_s, and ω_s' all change with the true anomaly during the whole orbital periods [2], and they can be respectively presented as:

$$R_s = \left[a\left(1-e^2\right)\right] / (1 + e\cos f) \tag{6}$$

$$R_s' = e\sin f \sqrt{\mu / [a\left(1-e^2\right)]} \tag{7}$$

$$R_s{}'' = \mu e\cos f (1 + e\cos f)^2 \Big/ \left[a^2\left(1-e^2\right)^2\right] \tag{8}$$

$$\omega_s = \sqrt{\mu / [a\left(1-e^2\right)]^3}\,(1 + e\cos f)^2 \tag{9}$$

$$\omega_s' = -2\mu e\sin f (1 + e\cos f)^3 \Big/ \left[a^3\left(1-e^2\right)^3\right] \tag{10}$$

When the satellite moves in the orbit, the radar beam center line intersects with the Earth surface to form a group of points, known as targets. As depicted in Fig. 2, the five state vectors of the targets are presented as follows, where the subscript t means targets.

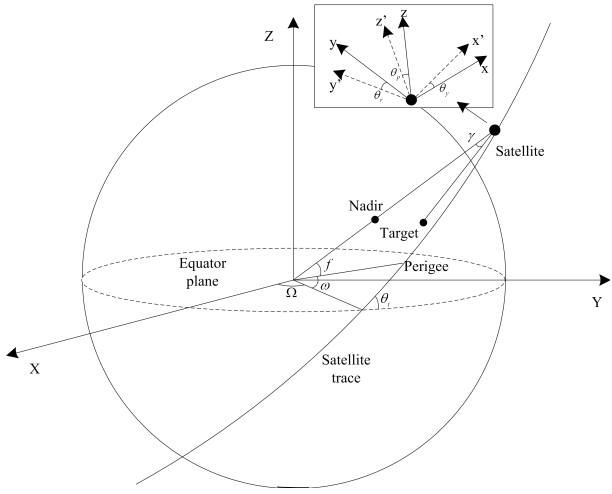

Figure 2. Geo-SAR geometry in 3D space.

$$\mathbf{r}_t = A_{re}A_{ea}\left(-r,0,0\right)^T + \mathbf{r}_s \tag{11}$$

$$\mathbf{v}_t = A_{rv}A_{vo}\begin{pmatrix} -\omega_e R_a \cos\theta_{lat}\sin\theta_{long} \\ \omega_e R_a \cos\theta_{lat}\cos\theta_{long} \\ 0 \end{pmatrix} \tag{12}$$

$$\mathbf{A}_t = A_{rv}A_{vo}\begin{pmatrix} -\omega_e^2 R_a \cos\theta_{lat}\cos\theta_{long} \\ -\omega_e^2 R_a \cos\theta_{lat}\sin\theta_{long} \\ 0 \end{pmatrix} \tag{13}$$

$$\mathbf{A}_t' = A_{rv}A_{vo}\begin{pmatrix} \omega_e^3 R_a \cos\theta_{lat}\sin\theta_{long} \\ -\omega_e^3 R_a \cos\theta_{lat}\cos\theta_{long} \\ 0 \end{pmatrix} \tag{14}$$

$$\mathbf{A}_t{}'' = A_{rv}A_{vo}\begin{pmatrix} \omega_e^4 R_a \cos\theta_{lat}\cos\theta_{long} \\ \omega_e^4 R_a \cos\theta_{lat}\sin\theta_{long} \\ 0 \end{pmatrix} \tag{15}$$

where A_{ea}, A_{re}, A_{rv} and A_{vo} are the Euler transformation matrixes:

$$A_{ea}=\begin{pmatrix} \cos\gamma & 0 & -k\sin\gamma \\ 0 & 1 & 0 \\ k\sin\gamma & 0 & \cos\gamma \end{pmatrix} \tag{16}$$

$$A_{re}=\begin{pmatrix} 1 & 0 & 0 \\ 0 & \cos\theta_y & \sin\theta_y \\ 0 & -\sin\theta_y & \cos\theta_y \end{pmatrix}\begin{pmatrix} \cos\theta_p & \sin\theta_p & 0 \\ -\sin\theta_p & \cos\theta_p & 0 \\ 0 & 0 & 1 \end{pmatrix}\begin{pmatrix} \cos\theta_r & 0 & -\sin\theta_r \\ 0 & 1 & 0 \\ \sin\theta_r & 0 & \cos\theta_r \end{pmatrix} \tag{17}$$

$$A_{rv}=\begin{pmatrix} \cos f & \sin f & 0 \\ -\sin f & \cos f & 0 \\ 0 & 0 & 1 \end{pmatrix} \tag{18}$$

$$A_{vo}=\begin{pmatrix} \cos\omega & \sin\omega & 0 \\ -\sin\omega & \cos\omega & 0 \\ 0 & 0 & 1 \end{pmatrix}\begin{pmatrix} 1 & 0 & 0 \\ 0 & \cos\theta_i & \sin\theta_i \\ 0 & -\sin\theta_i & \cos\theta_i \end{pmatrix}\begin{pmatrix} \cos\Omega & \sin\Omega & 0 \\ -\sin\Omega & \cos\Omega & 0 \\ 0 & 0 & 1 \end{pmatrix} \tag{19}$$

where ω_e is rotational angular velocity of the Earth, γ the elevation angle, θ_y the yaw angle, θ_p the pitch angle, and θ_r the roll angle, and k the beam pointing direction ($k = 1$ for right look, and $k = -1$ for left look). The value of r is the instantaneous range from sensor to targets, R_a the local Earth radii of the targets, and θ_{lat} and θ_{long} are respectively local latitudes and longitudes of the targets. The expressions of r, R_a, θ_{lat} and θ_{long} can be derived in the Earth centered inertial coordinates (ECI) directly. According to the discussions above, the sensor's coordinates in ECI is:

$$\begin{pmatrix} x_s \\ y_s \\ z_s \end{pmatrix} = \begin{pmatrix} R_s\cos\left(f+\omega\right) \\ R_s\sin\left(f+\omega\right)\cos\theta_i \\ R_s\sin\left(f+\omega\right)\sin\theta_i \end{pmatrix} \tag{20}$$

After a series of derivations, the coordinates of the targets in ECI can be expressed as:

$$\begin{pmatrix} X_t \\ Y_t \\ Z_t \end{pmatrix} = \begin{pmatrix} Ar + x_s \\ Br + y_s \\ Cr + z_s \end{pmatrix} \tag{21}$$

where A, B and C can be respectively given as:

$$\begin{aligned} A \;=\; & -\cos(f+\omega)\cos\theta_p\cos(\gamma+\theta_r) \\ & +\sin(f+\omega)\cos\theta_y\sin\theta_p\cos(\gamma+\theta_r) \\ & +k\sin(f+\omega)\sin\theta_y\sin(\gamma+\theta_r) \end{aligned} \tag{22}$$

$$\begin{aligned} B \;=\; & -\cos\theta_i\sin(f+\omega)\cos\theta_p\cos(\gamma+\theta_r) \\ & -\cos\theta_i\cos(f+\omega)\cos\theta_y\sin\theta_p\cos(\gamma+\theta_r) \\ & -k\cos\theta_i\cos(f+\omega)\sin\theta_y\sin(\gamma+\theta_r) \\ & -\sin\theta_i\sin\theta_y\sin\theta_p\cos(\gamma+\theta_r)+k\sin\theta_i\cos\theta_y\sin(\gamma+\theta_r) \end{aligned} \tag{23}$$

$$\begin{aligned} C \;=\; & -\sin\theta_i\sin(f+\omega)\cos\theta_p\cos(\gamma+\theta_r) \\ & -\sin\theta_i\cos(f+\omega)\cos\theta_y\sin\theta_p\cos(\gamma+\theta_r) \\ & -k\sin\theta_i\cos(f+\omega)\sin\theta_y\sin(\gamma+\theta_r) \\ & +\cos\theta_i\sin\theta_y\sin\theta_p\cos(\gamma+\theta_r)-k\cos\theta_i\cos\theta_y\sin(\gamma+\theta_r) \end{aligned} \tag{24}$$

As the Earth surface is modeled as an ellipsoid:

$$\frac{X_t^2}{R_e^2}+\frac{Y_t^2}{R_e^2}+\frac{Z_t^2}{R_p^2}=1 \tag{25}$$

where $R_e = 6378.137\,\text{km}$ and $R_p = 6356.752\,\text{km}$ are the equatorial and polar radii of the ellipsoidal Earth [1]. Substituting (21)–(24) into (25) and simplifying, r can be calculated as:

$$r=\frac{-K_2-\sqrt{K_2^2-4K_1K_3}}{2K_1} \tag{26}$$

where K_1, K_2 and K_3 can be given as:

$$\begin{cases} K_1 = R_p^2A^2+R_p^2B^2+R_e^2C^2 \\ K_2 = 2\left(Ax_sR_p^2+By_sR_p^2+Cz_sR_e^2\right) \\ K_3 = R_p^2x_s^2+R_p^2y_s^2+R_e^2z_s^2-R_e^2R_p^2 \end{cases}$$

Finally, the local latitudes, longitudes and Earth radii of the targets can be separately calculated as:

$$\theta_{lat} \;=\; \arctan\left[\frac{Z_t}{\sqrt{X_t^2+Y_t^2}}\right] \tag{27}$$

$$\theta_{long} \;=\; \Omega+\begin{cases} \arctan\left[Y_t/X_t\right], & (X_t>0, Y_t>0) \\ \arctan\left[Y_t/X_t\right]+2\pi, & (X_t>0, Y_t<0) \\ \arctan\left[Y_t/X_t\right]+\pi, & (X_t<0) \end{cases} \tag{28}$$

$$R_a = \sqrt{\frac{R_e^2 R_p^2}{\left[R_p \cos\theta_{lat}\right]^2 + \left[R_e \sin\theta_{lat}\right]^2}} \tag{29}$$

Substituting (26)–(29) into (11)–(15), the five state vectors of the targets can be obtained.

2.2. Doppler Parameter Calculation

This section gives a rigorous derivation of Doppler parameter expressions based on the geometry model above. The range vector from the target to the sensor in SLC can be given as:

$$\mathbf{r} = \mathbf{r}_s - \mathbf{r}_t \tag{30}$$

The expression (30) may be rewritten as:

$$r^2 = (\mathbf{r}_s - \mathbf{r}_t)(\mathbf{r}_s - \mathbf{r}_t) \tag{31}$$

Differentiating both sides of (31) with respect to time from the first-order to the fourth-order, we can get r', r'', $r^{(3)}$ and $r^{(4)}$. The 1–4th order Doppler parameters can then be presented as:

$$f_{dc} = -\frac{2r'}{\lambda} = -\frac{2}{\lambda}\frac{(\mathbf{r}_s - \mathbf{r}_t)(\mathbf{v}_s - \mathbf{v}_t)}{r} \tag{32}$$

$$f_{1r} = -\frac{2r''}{\lambda} = -\frac{2}{\lambda}\left[\frac{(\mathbf{v}_s - \mathbf{v}_t)^2}{r} + \frac{(\mathbf{A}_s - \mathbf{A}_t)(\mathbf{r}_s - \mathbf{r}_t)}{r} - \frac{\lambda^2 f_{dc}^2}{4r}\right] \tag{33}$$

$$f_{2r} = -\frac{2r^{(3)}}{\lambda} = -\frac{2}{\lambda}\left[\frac{3(\mathbf{v}_s - \mathbf{v}_t)(\mathbf{A}_s - \mathbf{A}_t)}{r} + \frac{(\mathbf{r}_s - \mathbf{r}_t)(\mathbf{A}'_s - \mathbf{A}'_t)}{r} - \frac{3\lambda^2 f_{dc} f_{1r}}{4r}\right] \tag{34}$$

$$f_{3r} = -\frac{2r^{(4)}}{\lambda} = -\frac{2}{\lambda}\left[\frac{3(\mathbf{A}_s - \mathbf{A}_t)^2}{r} + \frac{4(\mathbf{v}_s - \mathbf{v}_t)(\mathbf{A}'_s - \mathbf{A}'_t)}{r} + \frac{(\mathbf{r}_s - \mathbf{r}_t)(\mathbf{A}''_s - \mathbf{A}''_t)}{r} - \frac{3\lambda^2 f_{1r}^2}{4r} - \frac{\lambda^2 f_{dc} f_{2r}}{r}\right] \tag{35}$$

where λ is the radar wavelength. Substituting (1)–(5) and (11)–(15) into (32)–(35), the 1–4th order Doppler parameters can be calculated.

3. PERTURBATION OF ORBIT

Since the Earth is an oblate ellipsoid, bulging at the equator, with even higher order non-sphericity, the gravitation field on the sensor

can never be considered as a central one. As a result, the six orbital elements are affected by perturbation force, and the satellite trajectory is not a simple ellipse in an invariant plane. The J_2, J_3 and J_4 perturbation terms and their effect on the Doppler parameters are analyzed in this paper. The gravitational potential function of the Earth is written as [15]:

$$U = \frac{\mu}{r}\left[1 - \frac{J_2 R_e^2}{2R_s^2}\left(3\sin^2\varphi - 1\right) - \frac{J_3 R_e^3}{2R_s^3}\left(5\sin^3\varphi - 3\sin\varphi\right) - \frac{J_4 R_e^4}{8R_s^4}\left(35\sin^4\varphi - 30\sin^2\varphi + 3\right)\right] \tag{36}$$

where φ is the local latitude of nadir, and it is convenient to be expressed as follow:

$$\varphi = \arcsin\left[\sin\theta_i \sin(f + \omega)\right] \tag{37}$$

According to (36), the perturbation potential function due to the Earth's oblateness is given by:

$$U_P = U - \frac{\mu}{r} \tag{38}$$

The perturbation force of satellite at the corresponding orbital position can then be represented as:

$$\mathbf{F} = \mathrm{grad}\left(U_p\right) \tag{39}$$

Its influence upon the satellite orbit is illuminated by Kozai, and the periodic perturbations of the first order and secular perturbations up to the second order are derived. The symbol χ represents the six orbital elements (a, e, θ_i, Ω, ω and M). Based on the conclusion above, the expressions of the six orbital elements under perturbation force have the same form as Equation (40).

$$\chi_P(t) = \overline{\chi_0} + \chi_1(t - t_0) + \chi_2(t - t_0) + \chi_s^{(1)}(t) + \chi_L^{(1)}(t) \tag{40}$$

where $\chi_P(t)$ is the orbital element under perturbation force, $\overline{\chi_0}$ the mean orbital element value, $\chi_1(t - t_0)$ the first-order secular term, $\chi_2(t - t_0)$ the second-order secular term, $\chi_s^{(1)}(t)$ the first-order short periodic term, $\chi_L^{(1)}(t)$ the first-order long periodic term, t the orbital time, and t_0 the start time. As a result, the actual six orbital elements, which are under perturbation force, are denoted by $a_P(t)$, $e_P(t)$, $\theta_{iP}(t)$, $\Omega_P(t)$, $\omega_P(t)$ and $M_P(t)$ respectively.

According to the theory in Section 2, the state vectors of sensor and target are decided by the six orbit elements and radar's beam pointing direction. During one orbital period of the sensor, the accumulated changes of the state vectors due to the varieties of six

orbital elements can never be neglected. Assuming that the beam pointing direction is invariant, the state vectors depend on the six orbital elements only. The expression of the 1–4th order Doppler parameter of spaceborne SAR is given by:

$$f_{nrP} = \Psi_n \left[a_P(t), e_P(t), \theta_{iP}(t), \omega_P(t), \Omega_P(t), M_P(t) \right], \quad (n = 0, 1, 2, 3) \quad (41)$$

where f_{nrP} is the nth-order Doppler parameter (f_{0rP} means Doppler centroid, f_{dc}), the subscript P means "under perturbation force", and the symbol Ψ_n represents "function of some parameters". The error in percentage of f_{nr} can be calculated by:

$$E_{f_{nr}} = \frac{(f_{nrP} - f_{nr})}{f_{nrP}} \times 100, \quad (n = 0, 1, 2, 3) \quad (42)$$

The results will be simulated and analyzed in Section 5.

4. ATTITUDE STEERING

In addition to the orbital perturbation, the beam pointing also has an obvious effect on the Doppler parameters. Due to the Earth rotation and orbital eccentricity, the periodic yaw and pitch angle are generated. The attitude steering should be performed to get the zero Doppler centroid over the entire swath during the whole orbital periods. The approach proposed in [16] has a good effect on Geo-SAR. After attitude steering has been applied, the beam center line direction will be quite different, and the Doppler parameters change significantly. A block diagram of steps to calculate the spaceborne SAR's Doppler parameters is shown in Fig. 3.

5. SIMULATION RESULTS

The Doppler parameter calculation error caused by ignoring orbital perturbation is illustrated in Section 5.1. The simulation and comparison of 1–4th order Doppler parameters before and after attitude steering are described in Section 5.2. The effects on Doppler parameters caused by attitude control error are presented in Section 5.3. Since the Doppler parameter properties of Geo-SAR are quite different from those of Leo-SAR, the comparison between them is shown in this section. Without loss of generality, TerraSAR-X is chosen as an example of Leo-SAR [14]. The simulation parameters are listed in Table 1.

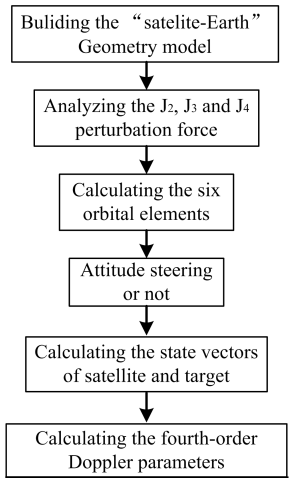

Figure 3. Doppler parameter calculation block diagram of spaceborne SAR.

Table 1. Simulation parameters.

Name	Geo-SAR	Leo-SAR
Orbital altitude (km)	35792	514
Inclination (°)	60	97.42
Elevation angle (°)	4.8	37.5
Wavelength (m)	0.24	0.03
Eccentricity	0.0011	
Longitude ascending node (°)	0	
perigee argument (°)	90	
J_2	1082.63×10^{-6}	
J_3	-2.5356×10^{-6}	
J_4	-1.62336×10^{-6}	

5.1. Calculation Errors Caused by Orbital Perturbation

The error analysis shows that the satellite elliptical trajectory in two-body condition could be mainly influenced by J_2, J_3 and J_4 perturbation terms. If the perturbation force is ignored, the 1–4th order Doppler parameters may have errors. Fig. 4 simulates the error in percentage of the four Doppler parameters of Geo-SAR and Leo-SAR.

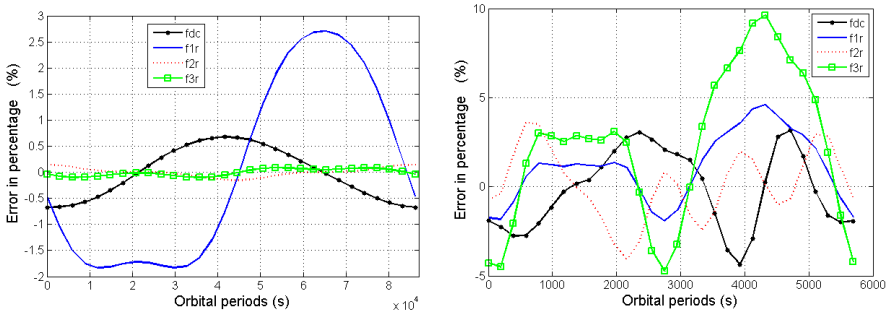

(a) Geo-SAR (b) Leo-SAR

Figure 4. Doppler parameter calculation error in percentage (Caused by ignoring the orbital perturbation).

As shown in Fig. 4(a), the perturbation force mainly has an effect on Doppler FM rate (f_{1r}) for Geo-SAR, and the largest error in percentage of f_{1r} is about 2.7%. Its influence on the other three Doppler parameters is not significant, however, small error in percentage below 0.7% can be observed. For Leo-SAR, the largest error in percentage of f_{3r} is about 9.8% and the errors of the other three Doppler parameters are all below 4.8%. Since the semi-major axis of Leo-SAR is around 1/6 of that of Geo-SAR, the perturbation force has effect on the six orbital elements tremendously for the former. As a result, it is reasonable that the calculation errors in percentage of Leo-SAR's Doppler parameters are larger than those of Geo-SAR's.

5.2. The Effect of Attitude Steering on Doppler Parameters

Since the beam pointing direction changes, the Doppler parameters may change significantly after attitude steering. The simulation results are depicted in Fig. 5.

In Fig. 5, it is obvious that the absolute values of Leo-SAR's Doppler parameters are larger than those of Geo-SAR's. In addition, the absolute values of Geo-SAR's change more sharply with respect to time. Besides the Doppler parameter properties of Leo-SAR and Geo-SAR are significantly different at the following two aspects:

- The Doppler centroid properties of both systems are similar, but the characteristics of f_{1r}, f_{2r} and f_{3r} are quite different.
- The attitude steering has an obvious effect on the values of f_{dc} and f_{2r} for both Leo-SAR and Geo-SAR. However, f_{1r} and f_{3r} are approximately independent of the beam pointing directions.

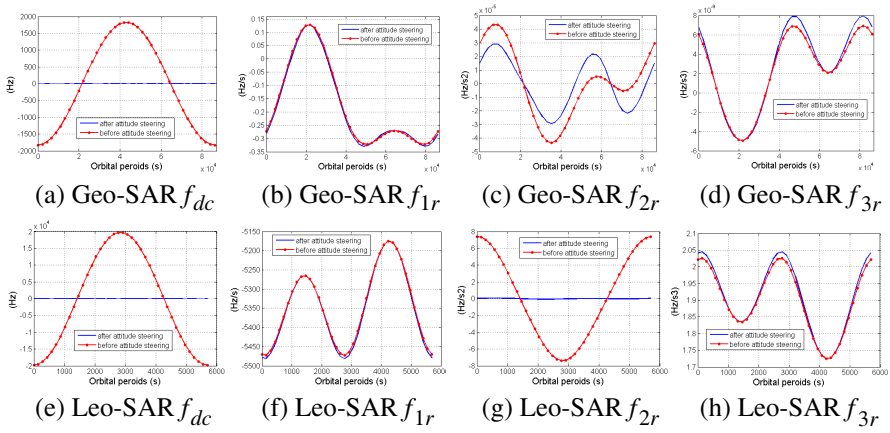

(a) Geo-SAR f_{dc} (b) Geo-SAR f_{1r} (c) Geo-SAR f_{2r} (d) Geo-SAR f_{3r}

(e) Leo-SAR f_{dc} (f) Leo-SAR f_{1r} (g) Leo-SAR f_{2r} (h) Leo-SAR f_{3r}

Figure 5. Doppler parameter properties comparison between Geo-SAR and Leo-SAR.

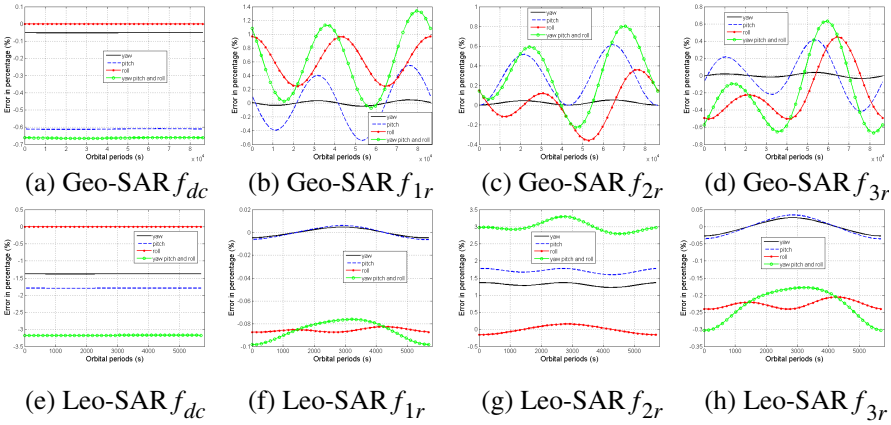

(a) Geo-SAR f_{dc} (b) Geo-SAR f_{1r} (c) Geo-SAR f_{2r} (d) Geo-SAR f_{3r}

(e) Leo-SAR f_{dc} (f) Leo-SAR f_{1r} (g) Leo-SAR f_{2r} (h) Leo-SAR f_{3r}

Figure 6. Doppler parameter error in percentage (Caused by attitude control error).

5.3. Attitude Control Accuracy

Any mispointing of radar beam, caused by the attitude control error, may lead to a shift of the Doppler parameters. The beam pointing errors of 0.05° for yaw, pitch and roll angles are assumed in this paper. The effects of pointing errors on the 1–4th order Doppler parameters for Geo-SAR and Leo-SAR are analyzed and simulated in Fig. 6.

According to the simulation results in Fig. 6, we can get the conclusions as follows:

- For a constant attitude control error, the error in percentage of Doppler centroid for Both Geo-SAR and Leo-SAR remains almost constant during the whole orbital periods. However, the errors of the other three Doppler parameters always change with time.
- All the errors of the three attitude angles could affect the Doppler parameters of the two spaceborne systems.
- The error of percentage of f_{dc} and f_{2r} for Leo-SAR are larger than those of Geo-SAR's, however, the pointing accuracy could have an obvious effect on the values of f_{1r} and f_{3r} for Geo-SAR.

6. CONCLUSION

It is necessary to obtain the accurate 1–4th order Doppler parameters for Geo-SAR. The calculation expressions of the Doppler parameters are derived based on an accurate geometry model. The J_2, J_3 and J_4 orbital perturbation terms could have an obvious influence on the trajectory of satellite. If the orbital perturbation force is ignored, the four Doppler parameters could have errors for both Geo-SAR and Leo-SAR. The largest error in percentage of Geo-SAR's Doppler parameters is about 2.7%. However, this value of Leo-SAR is around 9.8% since its orbital height is low and the effect of perturbation force is obvious. The absolute values of Doppler parameters of Geo-SAR are quite small and change evidently with respect to time compared with Leo-SAR. Besides the properties of them except the Doppler centroid frequency are quite different between Geo-SAR and Leo-SAR. For both Geo-SAR and Leo-SAR, f_{1r} and f_{3r} are approximately not affected by attitude steering, but the values of f_{dc} and f_{2r}, on the other hand, are sensitive to the satellite attitude. Finally, the attitude control error could also have an effect on the Doppler parameters for the two spaceborne SAR systems.

REFERENCES

1. Cumming, I. G. and F. H. Wong, *Digital Processing of Synthetic Aperture Radar Data: Algorithms and Implementation*, 113–168, Boston, Artech House, 2005.
2. Guo, D., H. Xu, and J. Li, "Extended wavenumber domain algorithm for highly squinted sliding spotlight SAR data processing," *Progress In Electromagnetics Research*, Vol. 114, 17–32, 2011.
3. Liu, Q., W. Hong, W. Tan, Y. Lin, Y. Wang, and Y. Wu, "An improved polar format algorithm with performance analysis

for geosynchronous circular SAR 2D imaging," *Progress In Electromagnetics Research*, Vol. 119, 155–170, 2011.

4. Tomiyasu, K., "Synthetic aperture radar in geosynchronous orbit," *Proc. Antennas and Propagation Society International Symposium*, USA, May 1978.
5. Tomiyasu, K. and J. L. Pacell, "Synthetic aperture radar imaging from an inclined geosynchronous orbit," *IEEE Trans. Geosci. Remote Sens.*, Vol. 21, No. 3, 324–328, 1983.
6. Wei, S. J., X. L. Zhang, and J. Shi, "Linear array SAR imaging via compressed sensing," *Progress In Electromagnetics Research*, Vol. 117, 299–319, 2011.
7. Xu, W., P. Huang, and Y.-K. Deng, "Muti-channel SPCMB-TOPS SAR for high-resolution wide-swath imaging," *Progress In Electromagnetics Research*, Vol. 116, 533–551, 2011.
8. Tan, W., W. Hong, Y. Wang, and Y. Wu, "A novel spherical-wave three-dimensional imaging algorithm for microwave cylindrical scanning geometries," *Progress In Electromagnetics Research*, Vol. 111, 43–70, 2011.
9. Zhang, M., Y. W. Zhao, H. Chen, and W.-Q. Jiang, "SAR imaging simulation for composite model of ship on dynamic ocean scene," *Progress In Electromagnetics Research*, Vol. 113, 395–412, 2011.
10. Li, F. K., D. N. Held, J. C. Curlander, and C. L. Wu, "Doppler parameter estimation for spaceborne synthetic aperture radar," *IEEE Trans. Geosci. Remote Sens.*, Vol. 23, No. 1, 47–56, 1985.
11. Raney, R. K., "Doppler properties of radars in circular orbits," *Int. J. Remote Sens.*, Vol. 7, No. 9, 1153–1162, 1986.
12. Raney, R. K., "A comment on Doppler FM rate," *Int. J. Remote Sens.*, Vol. 8, No. 7, 1091–1092, 1987.
13. Eldhuset, K., "A new fourth-order processing algorithm for spaceborne SAR," *IEEE Trans. Aero. Electronic Sys.*, Vol. 34, No. 3, 824–835, 1998.
14. Fielder, H., E. Boerner, J. Mittermayer, and G. Krieger, "Total zero Doppler steering: A new method for minimizing the Doppler centroid," *IEEE Geosci. Remote Sens. Lett.*, Vol. 2, No. 2, 141–145, 2005.
15. Kozai, Y., "The motion of a close earth satellite," *Astron. Journal*, Vol. 64, No. 9, 367–377, 1959.
16. Ze, Y., Z. Qing, C. Jie, and L. Sheng, "A new satellite attitude steering approach for zero Doppler centroid," *Proc. IET International Radar Conference*, Guilin, China, 2009.